Green hydrogen production via Reverse Electrodialysis and Assisted Reverse Electrodialysis Electrolyser: experimental analysis and preliminary economic assessment

Alessandra Pellegrino, Giovanni Campisi, Federica Proietto, Alessandro Tamburini*, Andrea Cipollina, Alessandro Galia, Giorgio Micale, Onofrio Scialdone

Dipartimento di Ingegneria, Università degli Studi di Palermo, viale delle scienze ed. 6, 90128 Palermo, Italy;

*Corresponding authors. E-mail: alessandro.tamburini@unipa.it

Abstract

In the climate changing context, hydrogen is leading the energy transition path. The present work focuses on the green hydrogen production exploiting salinity gradients via Reverse Electrodialysis (RED), in short circuit condition (REDsc), and Assisted RED (ARED), studied for the first time in hydrogen production as an improvement of the low current densities generated by RED. An extensive experimental campaign was carried out by feeding a RED stack with different salinity gradients and testing short-circuit-RED and Assisted-RED operative conditions. Hydrogen was produced successfully with ~100% Faradic Efficiency (FE) and productivity up to 1.7 mol h^{-1} m^{-2}. Also, the technology was compared with similar technologies and with the most established state-of-the-art electrolysers to identify advantages and disadvantages of the proposed route. Finally, a preliminary economic analysis was carried out and a minimum Levelized Cost of Hydrogen (LCOH) of 3.2 € kg^{-1}_{H2} was found, thus leaving room for further studies.

Keywords: electrolyser; electro-membrane processes; salinity gradient power; reverse electrodialysis; assisted reverse electrodialysis; H_2 production.

1. Introduction

The global energy consumption is expected to triple by 2050 because of the economic development of many countries and improvement of living standards [1]. The increase in global energy demand is not sustainable with the use of fossil fuels, and the new challenges must be overcome by promoting green and carbon-neutral technologies [2]. In addition, as highlighted in the latest global international meetings (G20 and COP27) the path to energy transition must be led also to curb the global warming [3,4]. With this respect, hydrogen is the most promising energy carrier that has been identified by world leaders as alternative to fossil fuels. European Commission has identified hydrogen as the key element through which European Union wants to reduce by 55 % greenhouse gases (GHG) emissions by 2030 [5], and to achieve the carbon-neutrality by 2050 [6]. Hydrogen can be produced in an eco-friendly way, with low-emission, and it can be used on a large global scale [7,8].

In 2021, global hydrogen demand reached 94 Mt, an increase of 3 Mt compared to 2019, when demand was the all-time high [9]. The hydrogen demand is still concentrated in the traditional applications of the refining and chemical sectors, however, the demand for new energy applications grew by 60 % in 2021 [9]. By 2030, it is estimated that hydrogen demand will reach about 180 million tonnes, of which almost half will come from new applications, particularly in power generation and hydrogen-based fuel production. The low-emission (blue and green) hydrogen production will account around 95 Mt, more than half of the global hydrogen production by 2030 [9]. About two-thirds of this production is based on the green hydrogen production through electrolysis, coupled with renewable resources; while another one-third is the blue hydrogen produced from fossil fuels with Carbon Capture Utilisation and Storage (CCUS) [9]. Focusing on the green hydrogen, the energy produced from renewable resources is stored in the form of hydrogen, in order to overcome the intrinsic discontinuity production of the renewable resources [10]. The green hydrogen is produced by electrolysis and more than 200 MW of electrolysers became operational in 2021, including 160 MW in China and more than 30 MW in Europe [9]. There are different types of electrolysers [11,12]: (i) Alkaline Electrolysers (AEL) [13] and (ii) Anionic Exchange Membrane Electrolysers (AEM)

[14], which are the most mature and widely used electrolysers; (iii) Proton Exchange Membrane Electrolysers (PEM) [15,16], which currently are the best performing; and (iv) Solid Oxide Electrolysis Cells (SOEC) [17], which are high-temperature and high-pressure electrolysers, still under development.

With this respect, new types of electrolysers have been developed, whose advancements are still at an early stage. In recent years, the combination of salinity gradient energy and green hydrogen production has been proposed: for instance, Reverse Electrodialysis (RED) has been adopted as a technology to be coupled with an electrolyser or as the electrolyser itself. The explanation of how the RED system works is reported in the *Supplementary materials – RED system*. RED is a technology that has several applications in addition to energy production, such as desalination of produced waters [18,19], energy storage [20,21], nano-/micro-fluidics [22], wastewater treatment [23,24], carbon dioxide reduction [25,26] and couplings with microbial fuel cells [27,28] or electrodialysis [29]. Energy production has been the most studied application so far: even, tests at pilot scale have been carried out in recent years.

Hydrogen production is one of the most recent RED applications. In 2014, among the first, Hatzell et al. [30] developed a new method to treat acid waste stream and improving the performance of the Ammonium Bicarbonate (AmB) RED system to capture waste heat energy. Specifically, hydrogen is produced in the system by consuming the acid to be disposed of at the cathode with 70.5 % ± 4 % maximum cathodic recovery of H_2. Similarly, using AmB solutions, Raka et al. [31] conducted thermally driven H_2 production via RED. They developed a model to estimate the feasibility of a RED-AmB producing H_2 at the cathode (productivity 1.19 mol m^{-2} h^{-1}) with low waste heat as thermal source. In 2017, Nazemi et al. [32] developed a thermodynamic model for RED to evaluate the electricity and hydrogen that can be obtained from the system from the natural mixing process of NaCl solutions, resulting in a productivity of 1.72 mol m^{-2} h^{-1} with a current of 11.5 mA cm^{-2}. Chen et al. [33] experimentally investigated the hydrogen production in a RED stack (by calling it REED, Reverse Electro-Electrodialysis). They used different concentration sets of diluted and concentrated

NaCl solutions, and the energy generated by the RED was partially consumed at the electrodes compartments since the system was coupled to a load. They obtained a hydrogen productivity of 0.55 mL cm^{-2} h^{-1} (0.25 mol m^{-2} h^{-1}) with a current density of 19.7 A m^{-2} coupled with cathodic Faradic Efficiency (FE / %) between 84 % and 96 %. Similarly, in 2019, Chen et al. [34] used a stack with one bipolar end-membrane that produced acid at the cathode. In this case, they obtained a H_2 productivity of 5.6 L m^{-2} h^{-1} (0.25 mol m^{-2} h^{-1}) with a FE of 91 % ± 6 %. Finally, the first pilot-scale applications were studied in 2018 by Tufa et al. [35] who adopted an RED pilot plant to supply energy to an AEL having a Specific Energy Consumption (SEC) of 56 kWh kg_{H2}^{-1}. In this system, the electrolyser worked at current densities of 88-110 mA cm^{-2} and an average H_2 productivity of 18 mol m^{-2} h^{-1} were obtained. In 2019, Higa et al. [36] tested a RED-H_2 pilot plant consuming partially of the energy generated by RED to produce green hydrogen at the cathode with a H_2 production rate of 0.9 L h^{-1} (H_2 productivity of 0.4 mol m^{-2} h^{-1}) and a FE of about 100 %.

The main limitation of RED-H_2 stacks concerns the low electric currents involved (i.e., low H_2 production rates). In the present work, the hydrogen production by RED was investigated with the main aim to increase the current densities and therefore the hydrogen productivity. Typically, the low current density is due to various causes including the low salinity gradients involved and the adopted operating conditions. As a matter of fact, RED systems are usually fed by river water-seawater and operated at the maximum power condition. This operating condition adopts an electric current being about equal to one-half of the short-circuit current, which, conversely, ideally would correspond to a doubled hydrogen production rate. Literature is lacking the combination of salinity gradient energy and green H_2 production at higher electric currents. This is why short circuit conditions were experimentally investigated in the present work, even with large salinity gradients (i.e., river water - brine). In addition, the experimental stack was operated under ARED conditions for the first time in order to further increase the green H_2 production rate. ARED, previously used for few applications including minerals recovery [37,38], wastewater treatment and CO_2 conversion [26], is able to boost the spontaneous ion fluxes of RED by connecting the stack with a power supply (instead of the

external load adopted in RED) (see Figure 1). Finally, a preliminary economic analysis was carried out to assess the economic feasibility of the proposed idea.

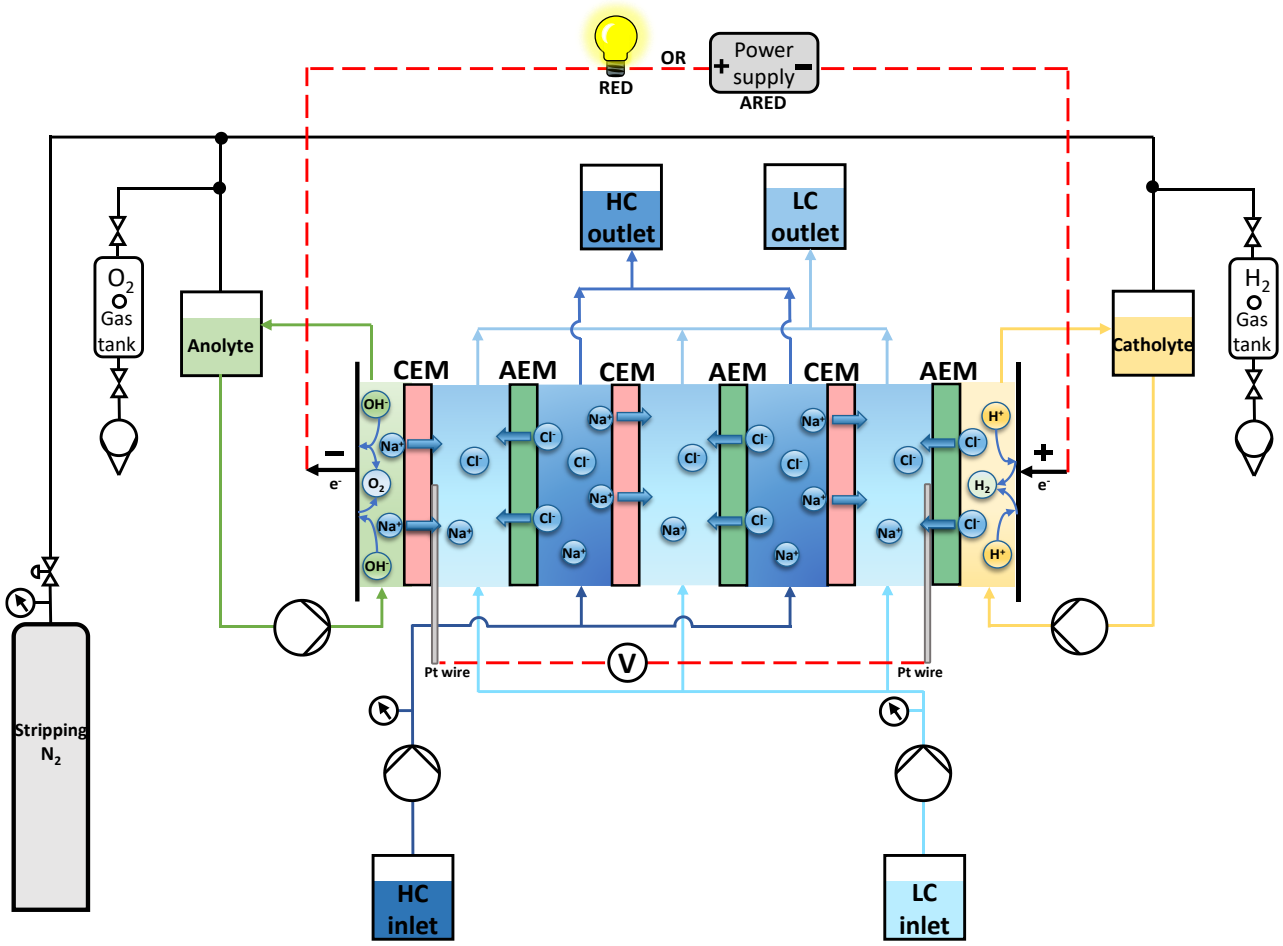

Figure 1. Experimental system used in the present work: ARED electrolyser.

2. Materials and Methods

In first instance, polarisation curves (in the *Supplementary materials*) were conducted to study how the system responds to the variations of the inlet concentrated solution. On these bases, two different sets of RED/ARED continuous tests were performed to measure the hydrogen produced with different concentrated solution as inlet. Linear Sweep Voltammetry characterizations were carried out to study specifically what occurred at the anode and understand how it may affect the system. To ensure test reproducibility, all tests were carried out at least twice under the same conditions.

2.1 Stack design and solutions

A co-current lab-scale RED unit with an active area of 10 x 10 cm^2 was used: it was equipped with 20 cell pairs of the commercial ion-exchange membranes Fujifilm Type 10 AEM and CEM (Tilburg, The Netherlands) and 300 μm thick woven spacers (Redstack, Sneek, The Netherlands).

During the stack assembly, two platinum wires were inserted into the last two salt compartments adjacent to the two end-membranes in order to measure the voltage of the cell pairs: the voltage loss at electrodes can be inferred from the difference of the external voltage minus the platinum wires one. The platinum wires were placed in contact with the end-membranes on the saline compartment-side, otherwise, on the electrode compartment-side these might be the site of electrode reactions.

Regarding the electrodes compartments, Ti mesh grid substrate with Pt/Ir ox (MMO – Mixed Metal Oxide) electrodes were used for both the anode and cathode on the base of the Sabatier volcano plot and the study on the best material for the hydrogen evolution reaction (HER) and the oxygen evolution reaction (OER) [39–42]. The catholyte was an aqueous solution of HCl 0.5 M and the anolyte was an aqueous solution of NaOH 0.5M, respectively prepared by diluting HCl (37 %, Merck) and NaOH pellets (98–100 %, Honeywell Fluka). The two end-membranes chosen were a Nafion CEM membrane for the anode, and an AEM Fujifilm Type 10 (Tilburg, The Netherlands) for the cathode. In addition, nitrogen (99.999 % purity; supplied by Air Liquide) was insufflate as stripping gas into the catholyte and the anolyte solutions tanks. The tests were carried out in continuous open-loop (i.e., once-through) mode, and the outlet flowrates from the anode and cathode compartments were measured using two Ki - Key Instrument LPM AIR 0.04-0.5 flow meters. Figure 1 shows the experimental set-up used.

NaCl (99.7% ChemSolute) was used to prepare the saline solutions. Two Leadfluid YT15 peristaltic pumps (BT601S, Lead Fluid Technology, CO LTD, China) were used to recirculate the anolyte and the catholyte solutions with a 525 mL min^{-1} flow rate, specifically, volumes of 150 mL and 200 mL of each solution were used, respectively. Two Cole-Parmer Masterflex I/P (77601-00, Illinois, USA) were used to pump the concentrated and diluted solutions with a flow rate of 180 mL min^{-1}. For both

the polarisation curves and the continuous RED/ARED tests, the concentrated and diluted salt solutions are fed in open-loop, to have the same electromotive force during the tests.

All the ARED tests were carried out by adopting a power supply (EA PS2042-10B, Elektro-Automatik GmbH & Co.KG) set in potentiostatic mode. In addition, two Fluke 175 multimeters were used to measure the external voltage and the cell pairs voltage, and a Fluke 8808A 5-1/2 Digit Multimeter was used to measure the current. The conductivities were measured for all the solutions, and the pH was measured using the pH-meter only for the salt solution, in particular a WTW conductivity and pH meter (WTW™ ProfiLine™ pH/Cond 3320 Universal Multi-parameter Portable) was used.

2.1.1 Continuous RED/ARED tests

The continuous RED and ARED tests were conducted in two different scenarios, with the same dilute stream, 1 g L^{-1} NaCl solution (river water) and two different concentrations of the concentrate: (i) 35 g L^{-1} NaCl (seawater), (ii) 300 g L^{-1} NaCl (bittern). The total duration of the tests using seawater and bittern as concentrate solutions was 240 and 120 minutes, respectively.

Each test was performed at a different current as summarized in Table 1. RED tests were carried out at short-circuit conditions (RED_{sc}), in which the external voltage was set to zero and the electromotive force generated by the RED unit was fully utilised in the system for hydrogen and oxygen production. The corresponding current is named I_{sc}. ARED tests were performed under different potentiostatic conditions by setting the voltage in order to obtain the desired current. Three different ARED operating conditions were tested: ARED 1, ARED 2 and ARED 3, depending on the different voltage set (ΔV_{ext}) (see Table 1). In the ARED 1 tests, the voltage was set in order to correspond to the short-circuit of the platinum wires: the external voltage was set to have a zero voltage at platinum wires (the corresponding current is named $I_{cell,sc}$). In other words, the difference between the external voltage and the cell pairs voltage (almost zero), which is the voltage consumed at the electrodes, was provided by the power supply. In the ARED 2 and ARED 3 tests, the voltage was set to obtain respectively twice and 2.5 times the short-circuit current of the stack (I_{sc}). In the results, the names of

the tests were expressed by the value of the concentrated solution used, followed by the type and the number of the test (e.g., 35 ARED 2).

Table 1. Overview of the test sets performed and their operating conditions.

Set 1	***35 RED$_{sc}$***	***35 ARED 1***	***35 ARED 2***	***35 ARED 3***
External Voltage set (ΔV_{ext} / V)	0.00	0.65	1.20	1.40
Desired Current	I_{SC}	$I_{cell,SC}$	I_{SC} x 2	I_{SC} x 2.5
Set 2	***300 RED$_{SC}$***	***300 ARED 1***	***300 ARED 2***	***300 ARED 3***
External Voltage set (ΔV_{ext} / V)	0	1	2.1	3.1
Desired Current	I_{SC}	$I_{cell,SC}$	I_{SC} x 2	I_{SC} x 2.5

In all tests, gases coming out of the catholyte and anolyte compartments were collected with a 250 µL gas-tight syringe (Hamilton Company Gastight 1725 TLL, Grisons, Switzerland) and they were analysed by gas chromatography using an Agilent 7890B GC equipped with a Supelco Carboxen-1000 (60/80) column and a thermal conductivity detector (TCD). Helium 99.999 % purity supplied from Air Liquide was used as carrier gas with constant pressure at 1 bar. Temperature program for the column was an isotherm at 35 °C for 5 min followed by 20 °C min^{-1} ramp up to 225 °C and by an isothermal step for 40 min; temperature of the TCD was 230 °C. In addition, a few millilitres of anolyte and catholyte were taken at regular intervals during the tests. Different analyses were carried out on these samples: (i) acid-base titration, to understand how the concentration of the electrolyte solutions varied; (ii) ion chromatography (Ion Chromatography Metrohm 882 Compact IC plus), to detect the amount of sodium and chloride ion concentrations diffused from the adjacent salt compartments; (iii) UV-Vis analysis to analyse any additional products. In particular, the Agilent cary 60 UV spectrophotometer by which the presence of hypochlorite in the anolyte solution was detected in some tests, obtaining a peak at the wavelength λ=291 nm: sodium hypochlorite 10 - 13 % (Sigma-Aldrich, Merk), was used for the calibration curve. Conductivity and pH were monitored in the diluted and concentrated solutions, using the conductivity and pH meter as described in section 2.1.

2.1.2 Test performance indicators

Faradic efficiency % (FE) was calculated in the continuous RED/ARED tests and it is the ratio between the charge used to obtain the product and the total charge circulating in the system (1):

$$Faradic\ Efficiency\ (FE)\ = \frac{z\ F\ mol_{prod}}{I\ t} 100\ [=]\ \% \qquad (1)$$

where mol_{prod} is the number of moles produced for a given product (i.e., H_2, O_2 or ClO^-) and t is the test duration. Productivity was also calculated in the continuous RED/ARED, and it is the quantity of product formed per hour and per electrode surface, as given by equation (2):

$$Productivity = 3600\ \frac{mol_{prod}}{t\ S_{electr}}\ [=] \frac{mol}{m^2\ h} \qquad (2)$$

The Specific Energy Consumption (SEC) represents the energy required to obtain 1 kg of the product of interest, in this case, hydrogen, as shown in equation (3):

$$SEC = \frac{1}{3600}\ \frac{\int_0^t U\ I\ dt}{mol_{H_2,t}\ MW_{H_2}} [=]\ \frac{kWh}{kg_{H_2}} \qquad (3)$$

2.1.3 Linear Sweep Voltammetry

Linear Sweep Voltammetry (LSV) tests were carried out to investigate in detail the anode reactions and how the variation in anolyte concentration during the tests affected the performances. The setup used consisted of an undivided electrodes cell with a Pt cathode and a Ti mesh substrate with Pt/Ir oxides (MMO – Mixed Metal Oxide) anode, working electrode, of the same type as the electrodes used in the stack. The anode surface area was 0.1 cm^2 to minimise ohmic losses. The reference electrode used is the Standard Calomel Electrode (SCE) but in the graphs of the results, the values had been shifted from the Standard Hydrogen Electrode (SHE). The LSV analyses were conducted with an AUTOLAB potentiostat - Metrohm (PGSTAT1, Utrecht, The Netherlands), and the voltage range analysed is up to 2.15 V vs SCE with a scan rate of 3 mV s^{-1}. Tests were carried out using different electrolyte solutions. A reference case was studied in which a 0.5 M NaOH solution was used, since this is the solution used as the starting anolyte for the stack tests. Subsequently, tests were

performed with the same concentration of NaOH, 0.5 M, and increasing concentrations of NaCl, 0.1 M, 0.2 M, 0.3 M and 0.5 M, in order to study how the presence of chloride affected the performance of the system. Then, a test was carried out with a 0.1 M NaOH and 0.2 M NaCl solution, representative of the anolyte solution obtained at the end of the RED/ARED continuous tests. Through this last LSV test, a comparison was made with the reference case with only NaOH, as they were representative of the evolution that the system underwent from the beginning to the end of the tests.

3 Results and discussion

3.1 Continuous RED/ARED tests with a low salinity gradient

Short-circuit RED (i.e., RED_{SC}) and ARED tests were performed at concentrations of NaCl of 35 and 1 g L^{-1} for the concentrate and diluted solutions, respectively (under the different potentiostatic conditions, as explained in the section 2.1.2, see Table 1). Figure 2 and Figure 3 show the corresponding output of currents and the fixed external voltage, respectively. As shown in Figure 2, the experiment carried out by RED in short-circuit conditions (35 RED_{SC} test) had the lowest current and it was constant during the test at approximately 0.2 A as expected from the polarisation curve in the *Supplementary material*. When external voltages (ΔV_{ext}) were applied to the stack (35 ARED tests) higher current densities were observed. These current values were not constant and slightly decrease during the tests. As the ΔV_{ext} applied increases, the difference between the initial and final current of each test was higher by 8, 13 and 19 % in the 35 ARED 1, 35 ARED 2 and 35 ARED 3 tests, respectively. The decrease in current during tests reflected the slight time variation of the cell pairs voltage reported in Figure 3.

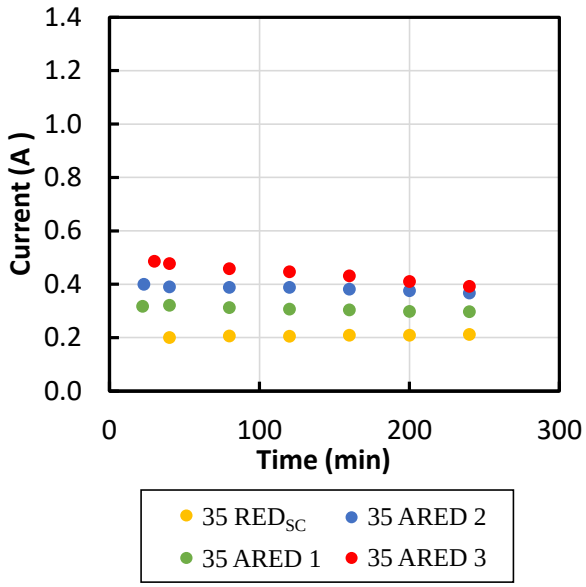

Figure 2. Electric current as a function of time. Tests with NaCl concentrations of 1 g L^{-1} for the dilute and 35 g L^{-1} for the concentrate solutions.

In fact, the 35 RED$_{SC}$ reported in Figure 3a shows that the gap between the external voltage and the platinum wires voltage was constant and approximately equal 0.67 V: it represented the voltage consumed at the electrodes. This value obtained experimentally was also found mathematically from Equation A.3 – Appendix 1, with a discrepancy between the two values of 3 %. Conversely, in the cases of 35 ARED tests, the voltage consumed at the electrodes increases since the beginning to the end of the tests. To rationalise these trends and study both the reactions which took place at the cathode and anode, gaseous and liquid products from both compartments were analysed.

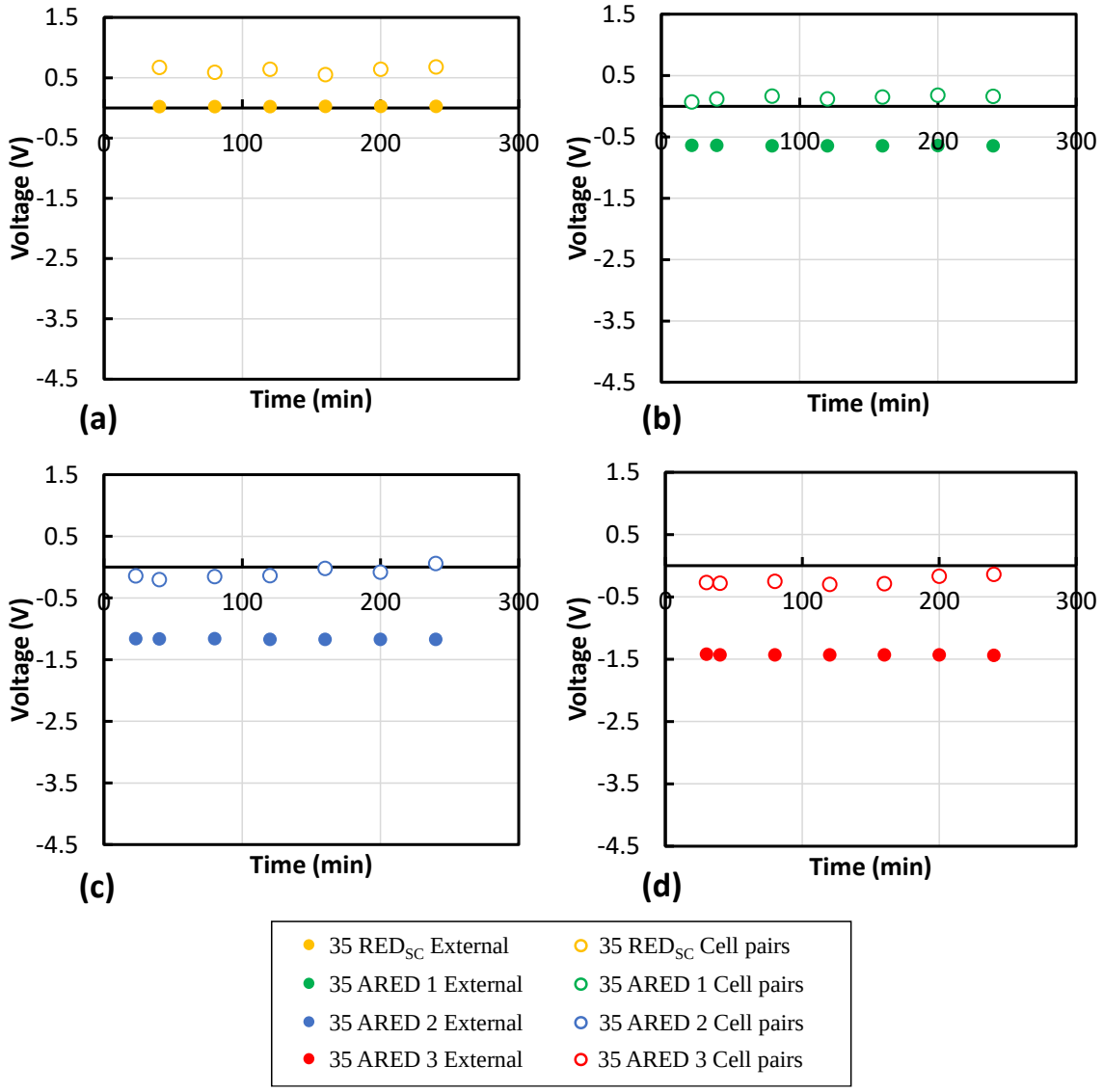

Figure 3. Tests with NaCl concentrations of 1 g L^{-1} for the dilute and 35 g L^{-1} for the concentrate solutions: (a) 35 REDSC; (b) 35 ARED 1 (c) 35 ARED 2 (d) 35 ARED 3. External voltage measured in RED or fixed in the potentiostatic tests in ARED and cell pairs voltage variation during the test, the difference between the two values is the voltage consumed at electrodes compartment.

At the cathode compartment, the catholyte concentration decreased from the initial value of 0.5 M to approximately 0.2 and 0.1 M in the case of 35 RED$_{SC}$ and 35 ARED tests, respectively. The H^+ partially diffused into the adjacent salt compartment (~15 %), and partially reacted to produce hydrogen. Figure 4 shows the hydrogen faradic efficiencies (FE_{H_2}) and productivities during 35 RED$_{SC}$ and 35 ARED tests. The FE_{H_2} was almost 100% as a confirmation that the H_2 production is the only cathodic reaction occurring (Figure 4). Furthermore, hydrogen productivity increased almost proportionally (linearly) with the current, it varied from a minimum of ~0.4 mol m^{-2} h^{-1} in the 35

RED_{SC} test with an uncertainty of ±0.066 mol m^{-2} h^{-1}, to a maximum of ~0.9 mol m^{-2} h^{-1} in the 35 ARED 3 test with an uncertainty of ±0.13 mol m^{-2} h^{-1} (Figure 4).

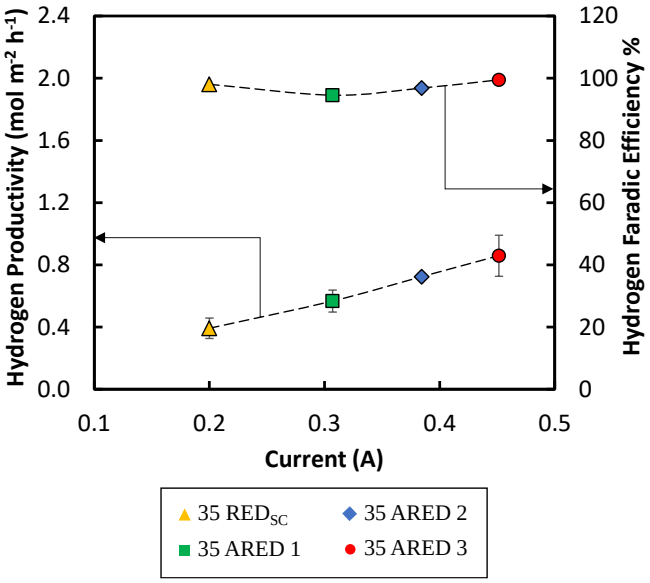

Figure 4. Hydrogen average faradic efficiencies and productivities versus the average current for each RED/ARED test performed with the concentrations of 1 g L^{-1} for the dilute and of 35 g L^{-1} for the concentrate.

Looking at the anode compartment in the same way, the anolyte NaOH concentration varied from an initial value of 0.5 M to a final value of 0.23 M in the 35 RED_{SC} test and to 0.1 M in the ARED tests. At the anode compartment, oxygen evolution was expected to be the main anodic process. Hence in the case of 35 RED_{SC} and 35 ARED 1 tests (ΔV_{ext} = 0 and ΔV_{ext}= 0.6V respectively), a FE of oxygen (FE_{O_2}) of approximately 99 % was observed. These results show that, in the cases of 35 RED_{SC} and 35 ARED 1 tests, oxygen evolution was the main reaction taking place at the anode (due to the water oxidation, reaction A2 in Appendix 1) and resulted in an almost constant current (Figure 2). Indeed, in 35 RED_{SC} and 35 ARED 1 tests, the ratio between the produced quantity of H_2 and O_2 (H_2/O_2) of 2:1 was maintained during the test, according to the reactions A1 and A2 (see Appendix 1). Conversely, when higher external voltages are used, a decrease of the FE_{O_2} was observed: 88 % in the 35 ARED 2 test (ΔV_{ext} = 1.2 V) and 76 % in the 35 ARED 3 test (ΔV_{ext} = 1.4 V), thus suggesting the occurrence of a competitive anodic reaction under these conditions. Hence, in these cases, the ratio H_2/O_2 was not 2. As expected, the application of the external voltage allowed to increase the

productivity of oxygen from 0.21 mol m^{-2} h^{-1} in 35 RED_{SC} to 0.28 and 0.32 mol m^{-2} h^{-1} in 35 ARED 1 and 35 ARED 2, respectively, due to the higher circulating current. Conversely, a slight decrease in productivity down to 0.29 mol m^{-2} h^{-1} was achieved at higher ΔV_{ext} in 35 ARED 3, because of the lower FE_{O_2} .

Table 2. Oxygen and hypochlorite productivities of the 35 RED_{SC}/ARED tests.

	35 RED$_{SC}$	***35ARED 1***	***35 ARED 2***	***35 ARED 3***
Oxygen productivity (mol m^{-2} h^{-1})	0.21	0.28	0.32	0.29
Hypochlorite productivity (mol m^{-2} h^{-1})	-	-	0.066	0.16

To clarify what happened under relatively high ΔV_{ext}, anolyte solutions were analyzed using UV-Visible spectroscopy. This investigation revealed the presence of hypochlorite (ClO^-) with concentrations of 0.017 M in 35 ARED 2 and 0.042 M in 35 ARED 3. In addition, by using the ion chromatography, the total quantity of chloride ions diffused from the salt compartment to the anolyte was found about 0.05 M in the 35 ARED 2 test and 0.08 M in the 35 ARED 3 test. These results could be rationalized by considering that, according to the literature [43], in presence of Cl^- and oxidative conditions, active chlorines could be produced at the anode due to the oxidation of chloride (eqs. (4) – (6)). The relative concentrations of Cl_2, HClO and ClO^- depend on the pH (Cl_2 at pH < 3.0, HClO at 3 ≤ pH ≤ 7.5 and ClO^- at pH >7.5, according to the Pourbaix diagram of the oxygen evolution reaction and chloride chemistry [43]). Hence, in our cases, the hypochlorite formation during the test was due to the anodic oxidation of chloride ions which diffused from the adjacent salt channels into the anode compartment.

pH<3 $$2Cl^- \leftrightarrow Cl_2 + 2e^- \quad (4)$$

3 ≤ pH ≤ 7.5 $$Cl^- + H_2O \leftrightarrow HClO + H^+ + 2e^- \quad (5)$$

pH >7.5 $$Cl^- + 2OH^- \leftrightarrow ClO^- + H_2O + 2e^-$$ (6)

At the anode side, the Hypochlorite Formation Reaction (HFR) was competitive with that of OER, and it was favoured under alkaline conditions. From these analyses, a hypochlorite FE (FE_{ClO^-}) of 9 % and 20 % was obtained in 35 ARED 2 and 35 ARED 3 tests, respectively, complementing the total FE of the anode compartment of approximately 100%. Table 2 reports the relative hypochlorite productivities which increased by increasing the applied ΔV_{ext}, as a consequence of the higher diffusive flux of chlorine ions from the adjacent dilute channel which concentrate more along the streamwise direction at large currents (Figure 2).

3.2 Continuous RED/ARED tests with a high salinity gradient

According to Table 1, RED/ARED continuous tests were carried out also with a concentration of the concentrated stream equal to 300 g L^{-1}, in order to increase the H_2 productivity. Figure 5 shows that a high salinity gradient in both RED and ARED conditions allowed to reach higher currents compared to the corresponding ones achieved using 35 g L^{-1}, as also evident from the polarisation curves in the *Supplementary material*. As already observed for the 35 g L^{-1} tests, also in this case, the larger the applied voltage, the sharper the current reduction over time. In particular, when higher currents were adopted, these decreased of ~28 % and 35 % over time (compared to the initial current) in the 300 ARED 2 and 300 ARED 3 tests, respectively.

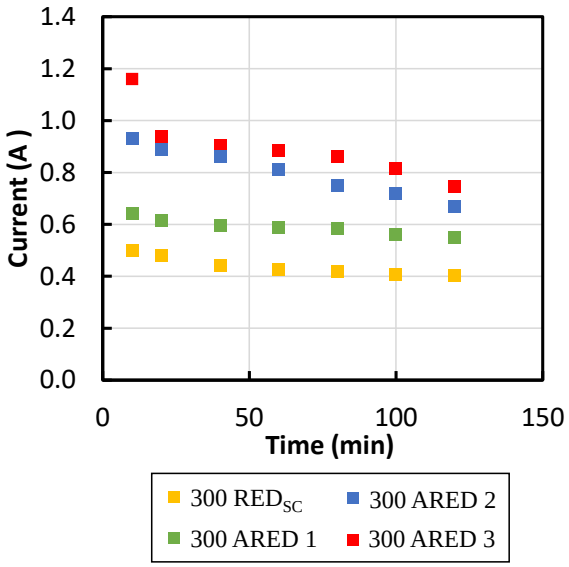

Figure 5. Electric current as a function of time. Tests with NaCl concentrations of 1 g L^{-1} for the dilute and 300 g L^{-1} for the concentrate.

This reflected the trend of the electrode voltage, which increased during time, as shown in Figure 6. In particular, the voltage consumed at the electrodes during the tests increased by ~25 % in the 300 ARED 1 (Figure 6b) and 300 ARED 2 (Figure 6c) tests, while in the 300 ARED 3 test (Figure 6d) it increased by ~88%. According to the results achieved under low salinity gradient, it might be stated that the higher the salinity gradient, the higher the concentration of the dilute channel next to the anodic compartment and, thus, the higher the Cl^- diffusion, thereby enhancing the HFR rate and hindering the OER at the anode.

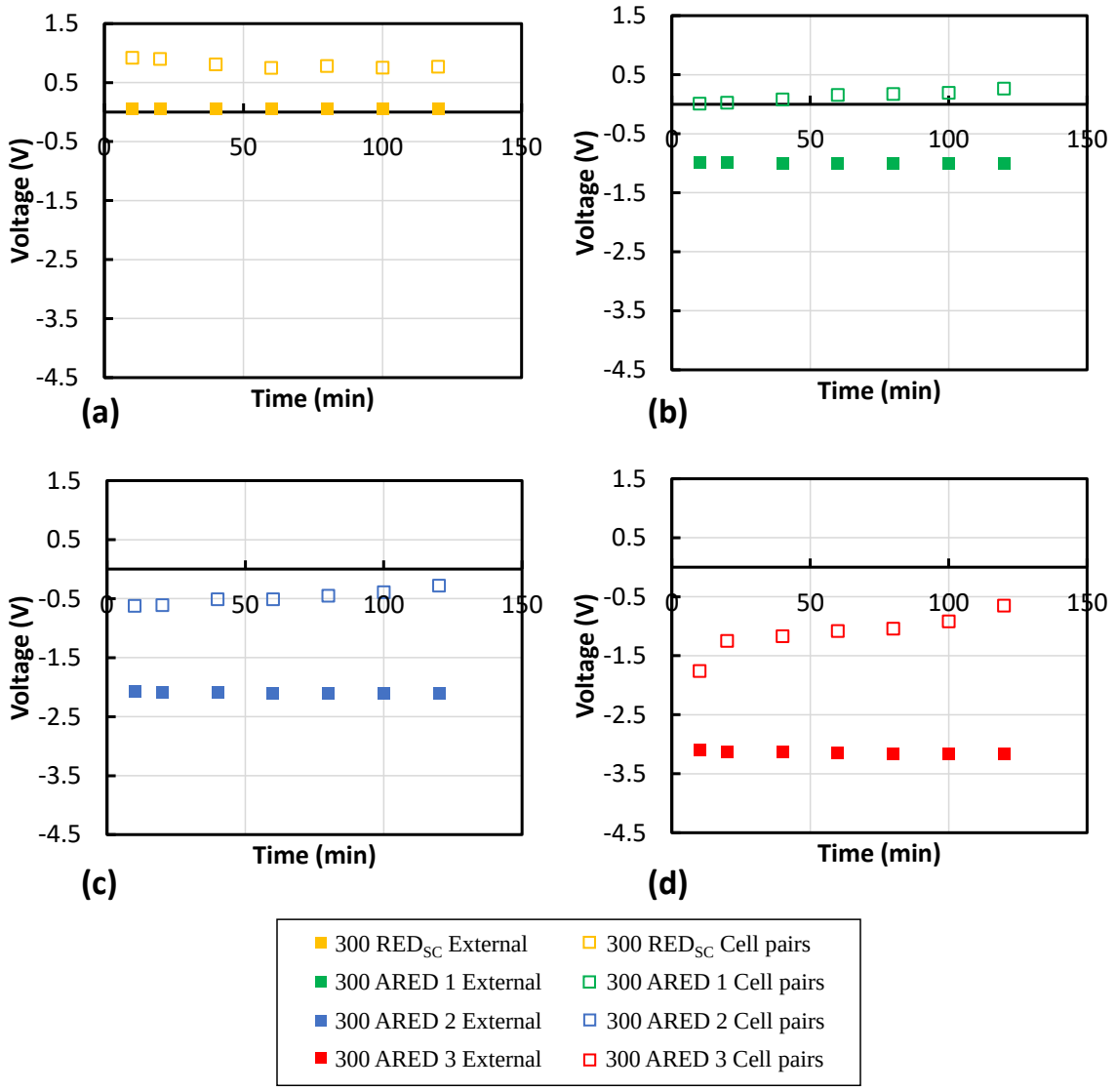

Figure 6. Tests with the concentrations of 1 g L^{-1} for the dilute and of 300 g L^{-1} for the concentrate: external voltage set in the potentiostatic tests and cell pairs voltage variation during the tests, the difference between the two values is the voltage consumed at electrodes compartment.

At the cathode compartment, the catholyte HCl was titrated, and during the tests, it varied the concentration from 0.5 M at the beginning of the tests, to 0.2 M at the end of the 300 RED$_{SC}$ test, to 0.05 M in the 300 ARED 3 test. In the other tests, the final concentrations obtained was in the range of these two values. As shown in Figure 7, FE_{H_2} is about 100 %, and the hydrogen productivity varied linearly with current, starting from of 0.84 mol m^{-2} h^{-1} in the 300 RED$_{SC}$ test with an uncertainty of ±0.045 mol m^{-2} h^{-1}, to the maximum achieved of 1.7 mol m^{-2} h^{-1} in the 300 ARED 3 test with an uncertainty of ±0.17 mol m^{-2} h^{-1}. In these tests, Faradic Efficiencies were almost equal to the tests with the 35 g L^{-1} concentrated solution, indicating that hydrogen production was optimal in both

cases. Productivity is therefore easily controlled by choosing the combination of concentrated solution used and power supply.

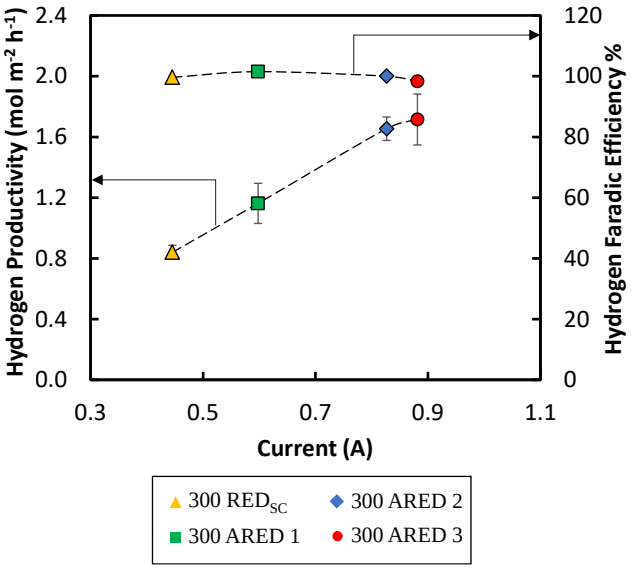

Figure 7. Hydrogen average faradic efficiencies and productivities *versus* the average current for each RED/ARED test performed with NaCl concentrations of 1 g L^{-1} for the dilute and of 300 g L^{-1} of the concentrate.

At the anodic compartment, the concentration of anolyte NaOH varied about in the same way as the catholyte, varying from an outlet concentration of 0.23 M in 300 RED_{SC} test to an outlet concentration of 0.06 M in the 300 ARED 3 test. In these cases, FE_{O_2} was 60 % and as expected also hypochlorite was formed, with a FE_{ClO^-} of 40 %. The oxygen and hypochlorite productivities of these tests are shown in Table 3.

Table 3. Oxygen and hypochlorite productivities of the 300 RED_{SC}/ARED tests.

	300 REDSC	***300 ARED 1***	***300 ARED 2***	***300 ARED 3***
Oxygen productivity (mol m^{-2} h^{-1})	0.24	0.33	0.4	0.43
Hypochlorite productivity (mol m^{-2} h^{-1})	0.37	0.47	0.69	0.82

As the Table 3 shows, the productivity of hypochlorite was higher than the oxygen one, but this was an expected result given: (i) the FE of the anodic process, which was 60% for oxygen and 40% for hypochlorite, and (ii) the number of electrons involved in the HFR which is half of the number of electrons involved in the oxygen evolution reaction. As expected, the chloride ions diffused were

higher than in the case of low concentrated salinity gradient and, in detail, the chloride concentration obtained in the anolyte compartment varied between 0.18 M and 0.26 M in all tests. Specifically, in the 300 RED_{SC}/ARED tests, the chloride ion diffusion was more than three times higher than in all 35 RED_{SC}/ARED tests, due to the higher concentration (by one order of magnitude) of the bittern chosen as the concentrate solution. The diffused chloride quantity was the key to understand the reason why the voltage consumed in the electrode compartments was higher in the 300 g L^{-1} tests. The anolyte and catholyte were recirculated in the system, so during the test, there was an accumulation of the diffused chloride, which was amplified where the diffusive flux was higher. In the test with 35 g L^{-1} as concentrate, as the diffused and accumulated chloride were lower, only a small hypochlorite quantity was formed in the tests with higher currents and with low FE (9% and 20%), probably due to issues relevant to kinetic mass transport control. In tests with a 300 g L^{-1} concentrated solution, there was the same ratio of FE_{O_2} (60%) to FE_{ClO^-} (40%) in all tests, indicative of the electrode selectivity in the absence of mass transport control. To better explain this aspect, it was very useful doing a comparison between 35 ARED 3 test and 300 RED_{SC} test. Both tests had the same electric current, an average value (from the beginning to the end of each test) of about 0.5 A. Using the same current, the two tests had the same FE_{H_2} and about the same hydrogen productivities (0.86 and 0.84 mol m^{-2} h^{-1}, for 35 ARED 3 and 300 RED_{SC} respectively). Notwithstanding having the same current, the two tests had different hypochlorite FEs 20% for the 35 ARED 3 test and 40% for the 300 RED_{SC} test, which meant oxygen FEs of 76% and 60% respectively. This meant that the amount of chloride ion diffused was a determinant factor in the anodic kinetic control, indeed in the two tests there was one order of magnitude difference in the total ion chloride diffused (i.e., 0.042 M in the 35 ARED 3 and 0.18 M in the 300 RED_{SC}).

3.3 Linear Sweep Voltammetry tests

To better understand the effect of NaCl on the oxygen evolution, a series of Linear Sweep Voltammetry (LSV) was performed using an electrolyte of 0.5M NaOH as reference solution and different concentrations of NaCl (from 0 to 0.5 M).

As shown in Figure 8a, when 0.1M or 0.2M NaCl was used, the polarization curves gave lower current densities with respect to that obtained in the absence of NaCl, at both low and high potentials. As explained by Scialdone et al. [44] in fact, in this case chloride was adsorbed on the anode surface, hindering the Oxygen Evolution Reaction (OER), and giving the Hypochlorite Formation Reaction (HFR). When the amount of chloride in solution increased (0.3 M and 0.5 M), two parts of the graph were distinguished: at low cell potentials and at high ones. At low potentials, the curves appeared shifted to the right, confirming the preponderant hindering action of the chloride against the OER. On the other hand, at high potentials, there was a cross of the curves with the reference test as the HFR started to be more favored. This behavior was also observed by Martinez-Huitle et al. [45] who used a Pt electrode, different from the one used in these tests which was mixed in Pt and Ir-ox. Martinez-Huitle et al. [45] similarly observed that Cl^- causes a shift of the OER and the solution had therefore a potentiostatic buffer effect at high chlorine concentrations.

In addition, a test was carried out with a different anolyte concentration in terms of OH^- and Cl^-, i.e., 0.1M NaOH and 0.2M NaCl (Figure 8). This concentration represented the average anolyte concentration at the end of the tests, and LSV was conducted with this solution to understand what changes between the start and end of the tests. As shown in Figure 8a, a more rightward-shifted curve was obtained, because the chloride concentration was higher than the hydroxyl ion concentration, so the hindering action of the chlorides was amplified. In addition, a plateau was observed towards the end of the test at high current densities, due to a mass transport control of the chloride ion on the electrode surface, after which the curve began to rise again. After the investigation of these LSV curves, it is appropriate to zoom on the low current density zone in which the RED and ARED tests were performed, as shown in Figure 8b.

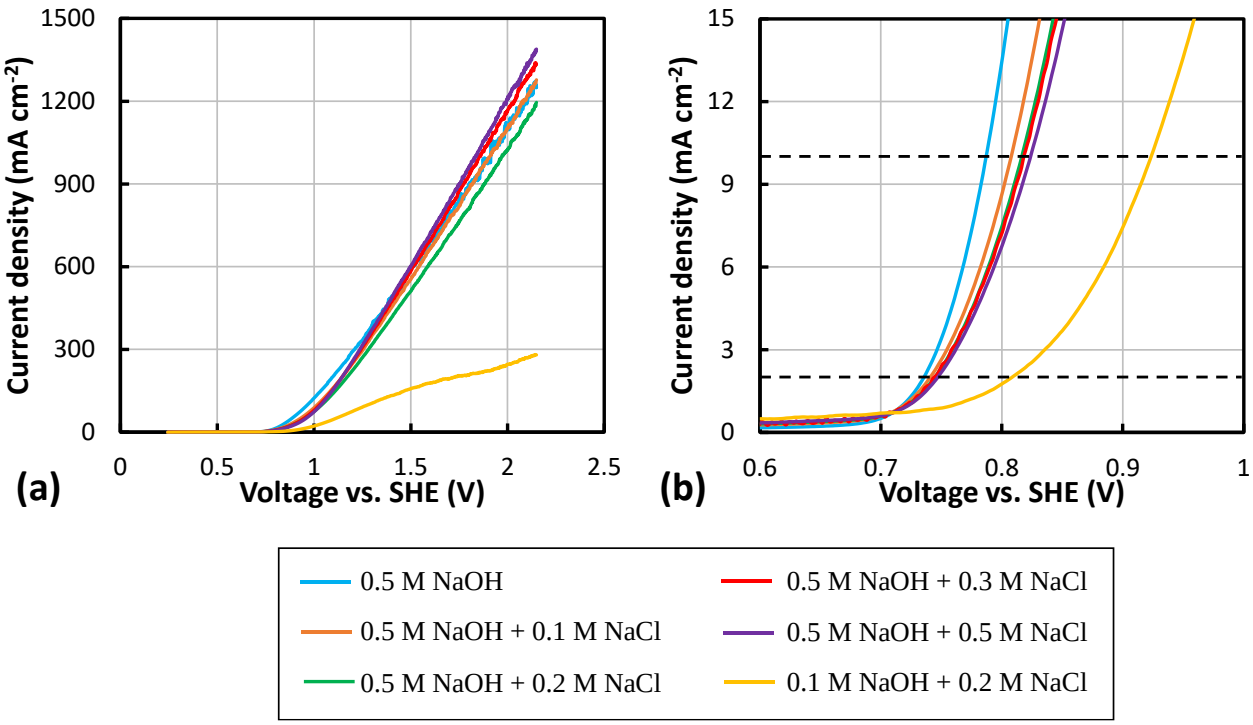

Figure 8. (a) Current density vs voltage, curves obtained with different concentration of NaOH and NaCl; (b) zoom at low current densities (a). Dashed lines indicate RED/ARED voltage investigated range.

The RED and ARED tests range from a minimum current density of 2 mA cm^{-2} (35 RED_{SC} test), to a maximum of approximately 10 mA cm^{-2} (300 ARED 3 test), a range highlighted between the dashed lines (Figure 8b). In this zoom, for the same potential there was a decrease of the current density produced between the start (reference light blue line 0.5 M NaOH) and the end of the tests (yellow 0.1 M NaOH + 0.2 M NaCl), due to the decrease in hydroxyl ions and the simultaneous increase in chloride ions. Furthermore, as the current increased, the curves representing the start and end of the tests were further apart, confirming the greater increase in voltage consumed at the electrodes seen in the experimental tests at higher current densities. The LSV analysis made it clear that the increase in the voltage consumed at the electrodes during the tests was caused by the presence of the chloride ion and its evolution into hypochlorite. However, it was not the only factor involved. As a matter of fact, it was experimentally observed that at high currents, the system was not able to effectively discharge the large number of gas bubbles produced. Some gas bubbles therefore remained trapped in the system, increasing its resistance and partially contributing to the increase in the voltage consumed at the electrode compartments.

3.4 Comparison with the RED-H_2 state of the art

The performances obtained in this work were compared with those achieved in other studies focused on the utilisation of RED technologies for hydrogen production. Table 4 shows a summary of the technology features and the performances obtained.

As the Table 4 shows, the data found in literature concern experimental applications performed mostly at laboratory scale. All experiments conducted at lab-scale were performed with stacks equipped with 20 cell pairs in order to have (i) a sufficiently high electromotive force and (ii) a negligible impact of ionic shortcut currents [46]. In all experiments, NaOH and HCl were identified as the most thermodynamically convenient anolyte and catholyte solutions, which were coupled to MMO electrodes with a titanium substrate and coated mostly with Pt and Ir, which better catalyse HER and OER reactions.

Table 4. Comparison of the main features of works devoted to green hydrogen production via salinity gradients technologies.

	Hatzell et al. [30]	***Chen et al.*** [33]	***35 (A)RED Electrolyser (this work)***	***300 (A)RED Electrolyser (this work)***	***Higa et al.*** [36]
Technology	AmB-RED	REED	Low conc. H_2 RED/ARED	High conc. H_2 RED/ARED	RED–H_2
Application	Lab-scale	Lab-scale	Lab-scale	Lab-scale	Pilot-scale
Cell pairs number	20	20	20	20	200
Anolyte used	1.4 M AmB/NaOH	0.5 M NaOH	0.5 M NaOH	0.5 M NaOH	5 % wt Na_2SO_4
Catholyte used	0.01 M AmB/HCl	2 – 0.2 M HCl	0.5 M HCl	0.5 M HCl	5 % wt Na_2SO_4
Electrodes material	Pt/Ir coated Ti electrode	Ru/Ir coated Ti electrode	Pt/Ir ox. coated Ti electrode	Pt/Ir ox. coated Ti electrode	Pt coated Ti electrode
Total membrane area (m^2)	0.87	0.756 (9x21 cm^2)	0.4 (10x10 cm^2)	0.4 (10x10 cm^2)	40 (20x50 cm^2)
Diluted solutions - LC	0.005 M AmB	0.008 – 0.5 M NaCl	0.017 M NaCl	0.017 M NaCl	~0.01/~0.02 M NaCl
Concentrated solutions - HC	1.4 M AmB	1.5 – 5 M NaCl	0.6 M NaCl	5.13 M NaCl	~0.6 M NaCl
Cell Temperature (°C)	40 – 60	25	25	25	18 – 28.5
Cell pressure (bar)	1	1	1	1	1
Current density ($A\ cm^{-2}$)	N.A.	Max. 0.002	0.002 – 0.005	0.005 – 0.01	0.0005 – 0.003
Cell Voltage (V)	N.A.	N.A.	0.02 – 1.4	0.04 – 3.1	N.A.
H_2 Faradic Efficiency (%)	70.5 ± 4 %	84 – 96 %	~97 %	~100 %	~100 %
Hydrogen Productivity	8.7 $m^3_{H2}\ m^{-3}\ day^{-1}$	0.55 mL $h^{-1}\ cm^{-2}$ (~0.25 mol $h^{-1}\ m^{-2}$)*	0.39 – 0.86 mol $h^{-1}\ m^{-2}$	0.84 – 1.7 mol $h^{-1}\ m^{-2}$	0.9 L h^{-1} (~0.4 mol $h^{-1}\ m^{-2}$)*
Anodic Faradic Efficiency (%)	N.A.	N.A.	OER: 99 – 76 % HFR: 0 – 20 %	OER: ~60 % HFR: ~40 %	N.A.
Anodic Productivity (mol $m^{-2}\ h^{-1}$)	N.A.	N.A.	OER: 0.21 – 0.29 HFR: 0 – 0.16	OER: 0.24 – 0.43 HFR: 0.37 – 0.82	N.A.

*conversions were made by the authors considering the molar standard volume of an ideal gas of 22.414 L mol^{-1}.

Analysing the current densities, Table 4 shows that the highest current densities were achieved in the present work, compared to both laboratory and pilot scale state of the art. In particular, current densities comparable to literature values were achieved in the 35 RED_{SC} test with a low salinity gradient, while higher values were reached in the boost tests using ARED operation mode. In the high salinity gradient tests, current density values higher than literature were already achieved in RED mode, while in the ARED configuration even higher values were achieved up to one order of magnitude. The faradic efficiencies of the present work are among the highest, and due to the combination with the higher current densities, the highest hydrogen productivities were achieved. At the same time, the faradic efficiencies of oxygen and hypochlorite with their respective productivities have been precisely quantified, as these can be products of relevant interest.

3.5 Comparison with the electrolysers state of the art

To complete the study, based on the voltage, current and hydrogen produced in each test, the Specific Energy Consumption was calculated and compared with other technologies reported in the literature (Figure 9); similarly, the principal data of each technology were summarised in Table 5.

Table 5. State-of-the-art for the features of Alkaline, PEM electrolysers and SOEC, compared with the (A)RED electrolyser proposed in this work.

	AEM Electrolyser [4,47]	***Alkaline Electrolyser*** [11,13,48–53]	***PEM Electrolyser*** [11,13,15,16,48–53]	***SOEC*** [11,13,17,48–54]	***35 (A)RED Electrolyser***	***300 (A)RED Electrolyser***
Electrolyte	DVB polymer support with KOH or $NaHCO_3$ 1 M [4]	Potassium hydroxide KOH 5-7 M [4]	PFSA membranes - water [4]	Yttria - stabilized Zirconia (YSZ) - steam [4]	Catholyte: 0.5 M HCl Anolyte: 0.5 M NaOH	Catholyte: 0.5 M HCl Anolyte: 0.5 M NaOH
Cell Temperature (°C)	40-60 [4]	70-90 [4]	50-80 [4,50]	700-850 [4]	25	25
Cell pressure (bar)	<35 [4,47]	<30 [4,47]	<70 [4,47]	<10 [4,47]	1	1
Current density (A cm^{-2})	0.2-2 [4,47]	0.2-0.8 [4,47]	0.6-2.0 [4,47]	0.3-1.0 [4,47]	0.002-0.005	0.005-0.01
Cell Voltage (V)	1.4-2.0 [4]	1.8-2.4 [15,49,51]	1.8-2.2 [15,49,51]	0.95-1.3 [15,49,51]	0.02-1.4	0.04-3.1

Electrode area (m^2)	<0.03 [4,47]	<3 [4,47,50]	<0.15 [47,52]	<0.02 [4,53]	0.01	0.01
Specific Energy Consumption ($kWh\ kg_{H2}^{-1}$)	51-66 [4,47]	47-66 [4,55]	47-63 [4,47,55]	42-52 [4,47,50,52,53]	0.6-39	1.4-85.7
Maturity	demonstration [4]	mature [52]	commercial [52]	demonstration [52]	first lab applications	first lab applications

As Table 5 shows, there are large differences between the technologies in the literature and the proposed technology. The operating conditions used in this first (A)RED Electrolyser were standard temperature and pressure. This represents an advantage, as the operation of other technologies at higher temperatures and pressures may imply a higher economic expenditure. By comparing current densities, the technology proposed in the present work exhibits values being one to two orders of magnitude lower. This is a significant drawback in terms of yearly productivity and currently represents the main limitation of this salinity gradient-based technology. On the other hand, the low current densities and the corresponding low SEC (Figure 9) were justified by the fact that the system consumes all the energy it self-generates. In RED tests, being short-circuited, the energy consumed is the total energy produced by the system, so the Specific Energy Consumption was close to zero: no power from the grid was used. In addition to consuming all the energy produced by the system, the ARED tests used an additional amount of energy taken from the grid through the power supply. Compared to the total energy consumed by the system, the energy taken from the grid varied from 16% to 32% in the 35 ARED tests, and from 20% to 43% in the 300 ARED tests. As Figure 9 shows, the SECs of the (A)RED electrolyser were always lower than the other technologies, except in the 300 ARED 3 test. This was due to the high concentration of chlorine in the bittern: there was the combined effect of higher chloride diffusion and higher hypochlorite formation, resulting in higher voltages reached during the test, as explained with the LSV curves. In all other tests, there was a great advantage in terms of SEC, which is one of the key performance indicators of the technology.

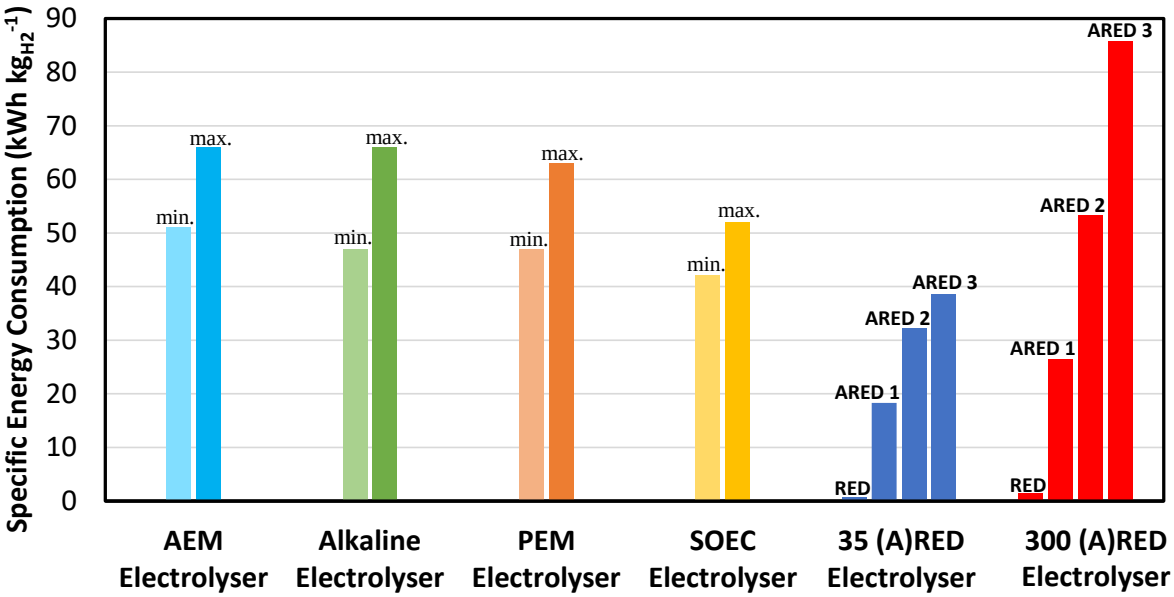

Figure 9. Specific Energy Consumption of the principal technologies: PEM and Alkaline electrolyser, the most widely used; SOEC those under greater development in recent years; (A)RED electrolyser with different concentrated solution (35 g L^{-1} and 300 g L^{-1}) and the same diluted solution (1 g L^{-1}), the technology proposed in this paper.

Among the advantages and disadvantages of the (A)RED Electrolyser compared to the state-of-the-art, the well-known low current density is the main limitation making the technology less competitive than conventional electrolysers. Considering this limit, an economic analysis is required in order to understand whether the present idea has anyhow the potential to be economically feasible. To this aim, a preliminary economic analysis of the (A)RED Electrolyser was conducted under the conditions tested experimentally to assess the relevant Levelized Cost of Hydrogen (LCOH).

3.6 Preliminary economic analysis results

A simplified mathematical model was developed to assess the main outputs of the (A)RED Electrolyser, such as the produced (RED) or consumed (ARED) electricity and the hydrogen productivity. The model was not spatially discretised, and the main characteristics were assumed to be constant and/or averaged along the main flow direction (lumped parameter model). The simplified model was inspired by semi-empirical models already validated in the literature [56,57]. The main difference concerned the modelling of the electrode compartments: traditionally, the voltage loss there was accounted for by the implementation of a suitable blank resistance. Conversely, in the present work, the presence of a no-reversible redox reaction at the electrodes required the

implementation of a suitable voltage loss calculation based on the thermodynamic potentials (~0.4 V), and the overvoltage, assumed with a conservatory value about 0.6 V. The technical model was found able to predict the experimental data: for example, in 35 RED_{SC}, the short-circuit current predicted by the model was 0.19 A while the experimental data was 0.2 A (5% discrepancy) and in 300 ARED 2 test, the experimental apparatus required 1.93 W, while the model estimation was about 2.02 W with an error of 4.79%.

The main characteristics of the stack and the scenario parameters chosen for the following economic analysis are shown in Table 6. The unit operated at the same conditions of the experimental campaign, e.g., flow rate, anolyte and catholyte solutions, feed solutions etc.

Table 6. Scenario parameters and features.

Membrane resistance	7	Ω cm^2
Membrane thickness	155	µm
Permselectivity	0.8	-
Salt diffusivity	4.52 $x10^{-12}$	m^2 s^{-1}
Electrode voltage drops	1[1]	V
Number of cell pairs	20	-
Length	1	m
Width	1	m
Spacers thickness	300	µm
Residence time per channel	20	s

[1]average value based on the experimental test results.

The results of the simplifying technical model were then used as input for a preliminary economic analysis. For such a plant, it was considered a lifetime of 20 years, a discount rate of 3% and a tax regime of 5% on the profit; in addition, a straight-line depreciation was used. The main economic parameters, costs (concerning both capital and operating expenditures) and prices are reported in Table 7.

Table 7. Main economic parameters, costs and prices.

Plant lifetime	20	Year
Discount rate	3	%
Working hour	8000	h $year^{-1}$

Tax	5	%
Membrane cost [18,58]	4	€ m^{-2}_{IEMS}
Membrane Lifetime	10	Year
Electrode cost	100	€ m^{-2}
Spacers cost [18,56]	2	€ m^{-2}_{IEMS}
Casing cost [18,56]	2	€ m^{-2}_{IEMS}
Labour cost [31]	10 % of equipment costs[2]	
Other costs [18]	3 % of FCI[3]	
Electricity cost [59]	0.1	€ kWh^{-1}
Anolyte and catholyte cost [59]	0.1	€ kg^{-1}
Oxygen price	0.1	€ kg^{-1}
Hydrogen price	variable	€ kg^{-1}

[2] the sum of the cost of the equipment costs (i.e., membranes, electrodes ect.)
[3] Fixed capital investment (i.e., equipment cost and labour cost)

The cash flow resulting from the economic analysis provided the Net Present Value (NPV), i.e., the cumulative amount of money obtained at the end of the plant lifetime. Hydrogen is the main product of the plant and NPV is strongly influenced by its selling price: a too low selling price of hydrogen made the NPV negative (no remuneration at the end of the plant life), whereas a higher price made the plant profitable. The Levelized Cost of Hydrogen (LCOH) is the specific selling price for hydrogen corresponding to a NPV equal to zero. Figure 10 shows the power density and the LCOH as a function of the electric current flowing into the system for the scenario described above. The power curves are shown in Figure 10a for the three different concentrated feed solutions: (i) the short-circuit current (triangle), (ii) the double of the short-circuit current (diamond) and (iii) the 2.5 times the I_{SC} (circle), according to the experimental campaign. These points were associated with the corresponding LCOH, in Figure 10b. As it can be seen, LCOH varied with current, but with different trends depending on the type of feed used. When using a feed of 35 g L^{-1}, i.e., seawater, the LCOH was among the highest, approaching 12 € kg^{-1}_{H2} in the case of the short-circuit, since the current produced was too low and, although no external energy was provided to the unit, the capital cost weighs heavily on the system, increasing the production cost for hydrogen. In short-circuit mode as the feed concentration increased, the corresponding current increased as well. At 300 g L^{-1}, LCOH decreased to a very competitive value of 3.2 € kg^{-1}_{H2}. This value is relevant to a future membrane cost of 4 € m^{-2}_{IEMs} (see Table 7). Interestingly, with a membrane cost of 10 € m^{-2}_{IEMs} this value would

increase to the still competitive value of 5.5 € kg^{-1}_{H2}. As the current increased (ARED), different trends were observed depending on the type of the feed. In the 35 g L^{-1} case, a minimum was reached at a current equal to twice the short-circuit current, a value that rises again at higher current values, due to the ohmic losses that became prominent. Conversely, in the 300 g L^{-1} case, LCOH increased almost linearly with the increase in the current flowing through the system, reaching an LCOH of more than 10 € kg^{-1}_{H2} for the 2.5x I_{SC} case.

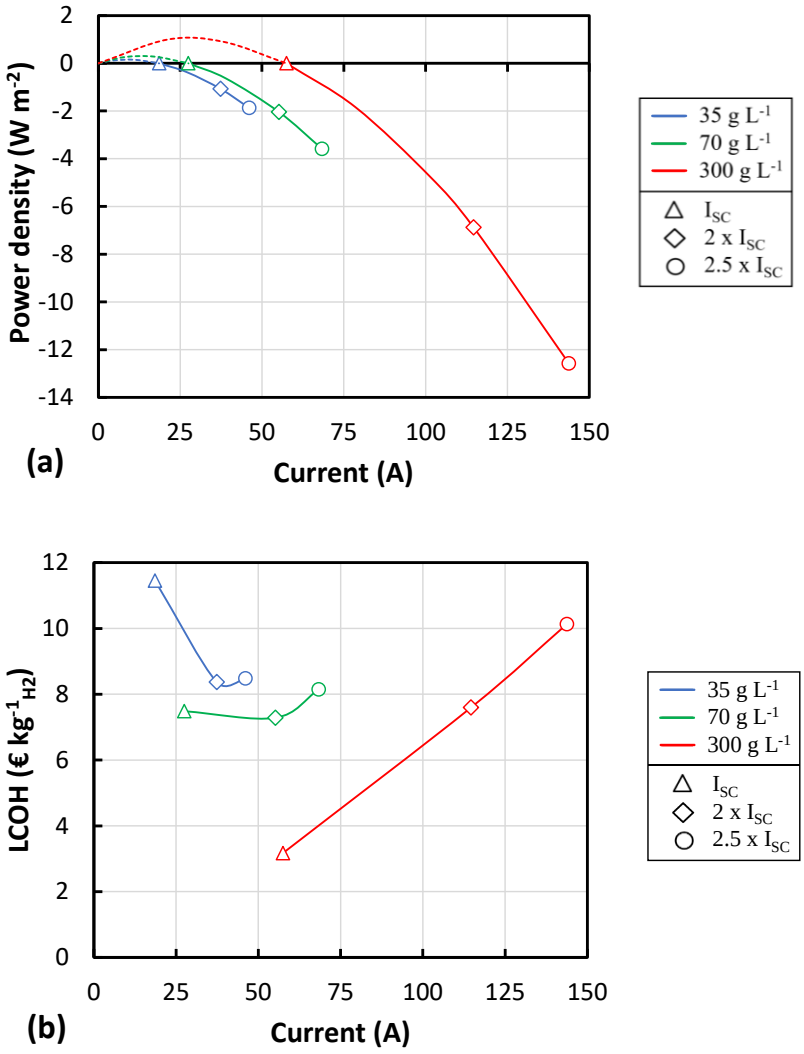

Figure 10. (a) Power curves versus the current, (b) LCOH trend versus the current for the three different concentrated feed solutions (35, 70 and 300 g L^{-1}). The dashed curves in (a) refers to RED mode, instead the continuous curves refers to ARED mode.

This preliminary economic analysis shows that, surprisingly, the cost of hydrogen production using an (A)RED unit is not prohibitive, and justifies the efforts devoted to further investigate this technology.

Conclusions

Hydrogen has been identified as the main alternative to the use of fossil fuels, for a green revolution. In particular, an emerging electrolyser, the (A)RED Electrolyser, has been comprehensively studied in the present work.

Specifically, an extensive experimental campaign was conducted with different concentrated solutions using different operational modes to characterize the system. Continuous tests were carried out under specific current conditions, such as RED short-circuit and different ARED conditions, testing the least and most concentrated concentrate solutions (35 and 300 g L^{-1}). The continuous tests resulted in almost maximum FE_{H_2} in all tests and hydrogen productivity varying linearly with current, from a minimum of 0.39 mol h^{-1} m^{-2} in the 35 RED test (I ~ 0.2 A) to a maximum of 1.7 mol h^{-1} m^{-2} in the 300 ARED 3 test (I ~ 1 A).

The study was completed by comparing the performance of the system with the salinity gradient Assisted RED electrolysers. It was found that under similar operating conditions, in the present work the highest currents for the technology were achieved, and consequently, the highest productivity was obtained. Nevertheless, a comparison with state-of-the-art electrolysers was carried out: it showed that these current densities were significantly lower than those relevant to typical electrolysers. Clearly, the same applies to the green hydrogen production rates. On the other hand, the salinity gradient energy exploitation allows an advantageous low SEC. With this respect, the preliminary economic analysis played a crucial role as it showed that, notwithstanding the low H_2 production rate of the technology, a minimum LCOH of 3.2 € kg^{-1}_{H2} in the 300 RED_{SC} condition might be potentially achievable. This value can be improved as the economic analysis considered the values experimentally obtained, which can be significantly enhanced. Also, no optimization was performed. This leaves room for further improvements and fully justify future efforts to be devoted to green H_2 production via salinity gradient energy assisted technologies.

Appendix 1

Voltage consumed at electrodes estimation

Considering the chosen catholyte (0.5 M HCl) and anolyte (0.5 M NaOH), the followed reactions (A.1) and (A.2) take place at the cathode and the anode of the system.

HER in acid medium: $2H^+ + 2e^- \leftrightarrow H_2 \qquad E^0 = 0\,V$ (A.1)

OER in alkaline/neutral medium: $4OH^- \leftrightarrow O_2 + 2H_2O + 4e^- \qquad E^0 = +0.4\,V$ (A.2)

On these bases, a mathematical estimation of the consumed voltage at the electrodes was calculated using equation (A.3), in which the thermodynamic contributions (E_{an}, (A.4) and E_{cat}, (A.5)) and the kinetic contribution from the well-known Butler and Volmer Equation (A.6) are present. For the calculations of anodic (η_{an}) and cathodic overvoltages (η_{cat}), the exchange current density values i_0 reported in the literature of 10^{-5} A m^{-2} and 8 A m^{-2} [60,61] were used respectively for the anodic and the cathodic calculations.

$$Voltage\ estimation = (E^0_{an} - E^0_{cat}) + \eta_{an} + \eta_{cat} \qquad \text{(A.3)}$$

$$E^0_{an} = 1.229 - 0.059\,pH \qquad \text{(A.4)}$$

$$E^0_{cat} = -0.059\,pH \qquad \text{(A.5)}$$

$$i = i_0 \left(\exp\left(\frac{\alpha F}{R T}\eta\right) - \exp\left(\frac{-(1-\alpha) F}{R T}\eta\right)\right) \qquad \text{(A.6)}$$

Glossary

Acronyms

AEL	Alkaline Electrolyser	LC	Low Concentrated
AEMEL	Anion Exchange Membrane Electrolyser	LSV	Linear Sweep Voltammetry
AEM	Anion Exchange Membrane	MMO	Mixed Metal Oxide
AmB	Ammonium Bicarbonate	OER	Oxygen Evolution Reaction

ARED	Assisted Reverse Electrodialysis	PEM	Proton Exchange Membrane Electrolyser
CEM	Cation Exchange Membrane	RED	Reverse Electrodialysis
CCUS	Carbon Capture Utilisation and Storage	REED	Reverse Electro-Electrodialysis
GHG	Greenhouse Gases	SCE	Standard Calomelan Electrode
HC	High Concentrated	SHE	Standard Hydrogen Electrode
HER	Hydrogen Evolution Reaction	SOEC	Solide Oxide Electrolysis Cell
HFR	Hypochlorite Formation Reaction	TCD	Thermal Conductivity Detector

Variables			
FE	Faradic Efficiency	NPV	Net Present Value
LCOH	Levelized Cost of Hydrogen	SEC	Specific Energy Consumption

Subscript			
ext	External	SC	Short Circuit
IEMs	Ionic Exchange Membranes		

References

[1] Global Energy Perspective 2022 Executive Summary, 2022.

[2] World Energy Outlook 2022, n.d. www.iea.org/t&c/.

[3] The Closing Window Climate crisis calls for rapid transformation of societies, 2022. https://www.unep.org/emissions-gap-report-2022.

[4] International Renewable Energy Agency, Green Hydrogen cost reduction scaling up electrolysers to meet 1.5 °C climate goal, 2020. www.irena.org/publications.

[5] J. Report prepared by the IED for the G20, The Future of Hydrogen, 2019.

[6] ENTEC Energy Transition Expertise Centre The role of renewable H_2 import & storage to scale up the EU deployment of renewable H_2, (n.d.). https://doi.org/10.2833/727785.

[7] D.J. Jovan, G. Dolanc, Can Green Hydrogen Production Be Economically Viable under Current Market Conditions, Energies (Basel). 13 (2020) 6599. https://doi.org/10.3390/en13246599.

[8] J.O. Abe, A.P.I. Popoola, E. Ajenifuja, O.M. Popoola, Hydrogen energy, economy and storage: Review and recommendation, Int J Hydrogen Energy. 44 (2019) 15072–15086. https://doi.org/10.1016/j.ijhydene.2019.04.068.

[9] IEA (2022), Hydrogen, Paris, n.d. https://www.iea.org/reports/hydrogen, License: CC BY 4.0.

[10] K.T. Møller, T.R. Jensen, E. Akiba, H. Li, Hydrogen - A sustainable energy carrier, Progress in Natural Science: Materials International. 27 (2017) 34–40. https://doi.org/10.1016/j.pnsc.2016.12.014.

[11] M.F. Ahmad Kamaroddin, N. Sabli, T.A. Tuan Abdullah, S.I. Siajam, L.C. Abdullah, A. Abdul Jalil, A. Ahmad, Membrane-Based Electrolysis for Hydrogen Production: A Review, Membranes (Basel). 11 (2021) 810. https://doi.org/10.3390/membranes11110810.

[12] S. Shiva Kumar, H. Lim, An overview of water electrolysis technologies for green hydrogen production, Energy Reports. 8 (2022) 13793–13813. https://doi.org/10.1016/j.egyr.2022.10.127.

[13] M. Mohebali Nejadian, P. Ahmadi, E. Houshfar, Comparative optimization study of three novel integrated hydrogen production systems with SOEC, PEM, and alkaline electrolyzer, Fuel. (2022). https://doi.org/10.1016/j.fuel.2022.126835.

[14] H.A. Miller, K. Bouzek, J. Hnat, S. Loos, C.I. Bernäcker, T. Weißgärber, L. Röntzsch, J. Meier-Haack, Green hydrogen from anion exchange membrane water electrolysis: A review of recent developments in critical materials and operating conditions, Sustain Energy Fuels. 4 (2020) 2114–2133. https://doi.org/10.1039/c9se01240k.

[15] M. Carmo, D.L. Fritz, J. Mergel, D. Stolten, A comprehensive review on PEM water electrolysis, Int J Hydrogen Energy. 38 (2013) 4901–4934. https://doi.org/10.1016/j.ijhydene.2013.01.151.

[16] T. Wang, X. Cao, L. Jiao, PEM water electrolysis for hydrogen production: fundamentals, advances, and prospects, Carbon Neutrality. 1 (2022) 21. https://doi.org/10.1007/s43979-022-00022-8.

[17] Y. Zhao, H. Xue, X. Jin, B. Xiong, R. Liu, Y. Peng, L. Jiang, G. Tian, System level heat integration and efficiency analysis of hydrogen production process based on solid oxide electrolysis cells, Int J Hydrogen Energy. 46 (2021) 38163–38174. https://doi.org/10.1016/j.ijhydene.2021.09.105.

[18] G. Campisi, A. Cosenza, F. Giacalone, S. Randazzo, A. Tamburini, G. Micale, Desalination of oilfield produced waters via reverse electrodialysis: A techno-economical assessment, Desalination. 548 (2023) 116289. https://doi.org/10.1016/j.desal.2022.116289.

[19] A. Cosenza, G. Campisi, F. Giacalone, S. Randazzo, A. Cipollina, A. Tamburini, G. Micale, Power Production from Produced Waters via Reverse Electrodialysis: A Preliminary Assessment, Energies (Basel). 15 (2022) 4177. https://doi.org/10.3390/en15114177.

[20] W.J. van Egmond, U.K. Starke, M. Saakes, C.J.N. Buisman, H.V.M. Hamelers, Energy efficiency of a concentration gradient flow battery at elevated temperatures, J Power Sources. 340 (2017) 71–79. https://doi.org/10.1016/j.jpowsour.2016.11.043.

[21] A. Cipollina, G. Micale, Sustainable Energy from Salinity Gradients, Woodhead Publishing, 2016.

[22] L. Cao, W. Guo, W. Ma, L. Wang, F. Xia, S. Wang, Y. Wang, L. Jiang, D. Zhu, Towards understanding the nanofluidic reverse electrodialysis system: Well matched charge selectivity

and ionic composition, Energy Environ Sci. 4 (2011) 2259–2266. https://doi.org/10.1039/c1ee01088c.

[23] P. Ma, X. Hao, A. Galia, O. Scialdone, Development of a process for the treatment of synthetic wastewater without energy inputs using the salinity gradient of wastewaters and a reverse electrodialysis stack, Chemosphere. 248 (2020) 125994. https://doi.org/10.1016/j.chemosphere.2020.125994.

[24] A. D'Angelo, M. Tedesco, A. Cipollina, A. Galia, G. Micale, O. Scialdone, Reverse electrodialysis performed at pilot plant scale: Evaluation of redox processes and simultaneous generation of electric energy and treatment of wastewater, Water Res. 125 (2017) 123–131. https://doi.org/10.1016/j.watres.2017.08.008.

[25] H. Wang, J. Yan, W. Song, C. Jiang, Y. Wang, T. Xu, Ion exchange membrane related processes towards carbon capture, utilization and storage: Current trends and perspectives, Sep Purif Technol. 296 (2022) 121390. https://doi.org/10.1016/j.seppur.2022.121390.

[26] P. Ma, X. Hao, F. Proietto, A. Galia, O. Scialdone, Assisted reverse electrodialysis for CO2 electrochemical conversion and treatment of wastewater: A new approach towards more eco-friendly processes using salinity gradients, Electrochim Acta. 354 (2020) 136733. https://doi.org/10.1016/j.electacta.2020.136733.

[27] A. D'Angelo, A. Galia, O. Scialdone, Cathodic abatement of Cr(VI) in water by microbial reverse-electrodialysis cells, Journal of Electroanalytical Chemistry. 748 (2015) 40–46. https://doi.org/10.1016/j.jelechem.2015.04.010.

[28] S. Pandit, C. Pandit, A. Singh Mathuriya, D.A. Jadhav, Blue energy meets green energy in microbial reverse electrodialysis cells: Recent advancements and prospective, Sustainable Energy Technologies and Assessments. 57 (2023) 103260. https://doi.org/10.1016/j.seta.2023.103260.

[29] Y. Mei, C.Y. Tang, Recent developments and future perspectives of reverse electrodialysis technology: A review, Desalination. 425 (2018) 156–174. https://doi.org/10.1016/j.desal.2017.10.021.

[30] M.C. Hatzell, X. Zhu, B.E. Logan, Simultaneous hydrogen generation and waste acid neutralization in a reverse electrodialysis system, ACS Sustain Chem Eng. 2 (2014) 2211–2216. https://doi.org/10.1021/sc5004133.

[31] Y.D. Raka, H. Karoliussen, K.M. Lien, O.S. Burheim, Opportunities and challenges for thermally driven hydrogen production using reverse electrodialysis system, Int J Hydrogen Energy. 45 (2020) 1212–1225. https://doi.org/10.1016/j.ijhydene.2019.05.126.

[32] M. Nazemi, J. Zhang, M.C. Hatzell, Harvesting Natural Salinity Gradient Energy for Hydrogen Production Through Reverse Electrodialysis Power Generation, Journal of Electrochemical Energy Conversion and Storage. 14 (2017). https://doi.org/10.1115/1.4035835.

[33] X. Chen, C. Jiang, Y. Zhang, Y. Wang, T. Xu, Storable hydrogen production by Reverse Electro-Electrodialysis (REED), J Memb Sci. 544 (2017) 397–405. https://doi.org/10.1016/j.memsci.2017.09.006.

[34] X. Chen, C. Jiang, M.A. Shehzad, Y. Wang, H. Feng, Z. Yang, T. Xu, Water-dissociation-assisted electrolysis for hydrogen production in a salinity power cell, ACS Sustain Chem Eng. 7 (2019) 13023–13030. https://doi.org/10.1021/acssuschemeng.9b02131.

[35] R.A. Tufa, J. Hnát, M. Němeček, R. Kodým, E. Curcio, K. Bouzek, Hydrogen production from industrial wastewaters: An integrated reverse electrodialysis - Water electrolysis energy system, J Clean Prod. 203 (2018) 418–426. https://doi.org/10.1016/j.jclepro.2018.08.269.

[36] M. Higa, T. Watanabe, M. Yasukawa, N. Endo, Y. Kakihana, H. Futamura, K. Inoue, H. Miyake, J. Usui, A. Hayashi, M. Matsuhashi, Sustainable hydrogen production from seawater and sewage treated water using reverse electrodialysis technology, Water Pract Technol. 14 (2019) 645–651. https://doi.org/10.2166/wpt.2019.048.

[37] A. Filingeri, M. Philibert, E. Filloux, N. Moe, A. Poli, A. Tamburini, A. Cipollina, Valorization of surface-water RO brines via Assisted-Reverse Electrodialysis for minerals recovery: Performance analysis and scale-up perspectives, Desalination. 541 (2022) 116036. https://doi.org/10.1016/j.desal.2022.116036.

[38] M. Vanoppen, E. Criel, G. Walpot, D.A. Vermaas, A. Verliefde, Assisted reverse electrodialysis—principles, mechanisms, and potential, NPJ Clean Water. 1 (2018) 9. https://doi.org/10.1038/s41545-018-0010-1.

[39] A. Lasia, Hydrogen evolution reaction, in: Handbook of Fuel Cells, John Wiley & Sons, Ltd, Chichester, UK, 2010. https://doi.org/10.1002/9780470974001.f204033.

[40] P. Quaino, F. Juarez, E. Santos, W. Schmickler, Volcano plots in hydrogen electrocatalysis-uses and abuses, Beilstein Journal of Nanotechnology. 5 (2014) 846–854. https://doi.org/10.3762/bjnano.5.96.

[41] S. Trasatti, Work function, electronegativity, and electrochemical behaviour of metals iii. electrolytic hydrogen evolution in acid solutions, Electroanalytical Chemistry and Interfacial Electrochemistry. 39 (1972) 163–184.

[42] N.T. Suen, S.F. Hung, Q. Quan, N. Zhang, Y.J. Xu, H.M. Chen, Electrocatalysis for the oxygen evolution reaction: Recent development and future perspectives, Chem Soc Rev. 46 (2017) 337–365. https://doi.org/10.1039/c6cs00328a.

[43] S. Dresp, F. Dionigi, M. Klingenhof, P. Strasser, Direct Electrolytic Splitting of Seawater: Opportunities and Challenges, ACS Energy Lett. 4 (2019) 933–942. https://doi.org/10.1021/acsenergylett.9b00220.

[44] O. Scialdone, S. Randazzo, A. Galia, G. Silvestri, Electrochemical oxidation of organics in water: Role of operative parameters in the absence and in the presence of NaCl, Water Res. 43 (2009) 2260–2272. https://doi.org/10.1016/j.watres.2009.02.014.

[45] C.A. Martínez-Huitle, S. Ferro, A. De Battisti, Electrochemical Incineration in the Presence of Halides, Electrochemical and Solid-State Letters. 8 (2005) D35. https://doi.org/10.1149/1.2042628.

[46] A. Culcasi, L. Gurreri, A. Zaffora, A. Cosenza, A. Tamburini, A. Cipollina, G. Micale, Ionic shortcut currents via manifolds in reverse electrodialysis stacks, Desalination. 485 (2020) 114450. https://doi.org/10.1016/j.desal.2020.114450.

[47] M. Chatenet, B.G. Pollet, D.R. Dekel, F. Dionigi, J. Deseure, P. Millet, R.D. Braatz, M.Z. Bazant, M. Eikerling, I. Staffell, P. Balcombe, Y. Shao-Horn, H. Schäfer, Water electrolysis: from textbook knowledge to the latest scientific strategies and industrial developments, Chem Soc Rev. 51 (2022) 4583–4762. https://doi.org/10.1039/d0cs01079k.

[48] Y. Naimi, A. Antar, Hydrogen Generation by Water Electrolysis, in: Advances In Hydrogen Generation Technologies, InTech, 2018. https://doi.org/10.5772/intechopen.76814.

[49] R. Bhandari, C.A. Trudewind, P. Zapp, Life cycle assessment of hydrogen production via electrolysis - A review, J Clean Prod. 85 (2014) 151–163. https://doi.org/10.1016/j.jclepro.2013.07.048.

[50] T. Smolinka, M. Günther, "Stand und Entwicklungspotenzial der Wasserelektrolyse zur Herstellung von Wasserstoff aus regenerativen Energien" Kurzfassung des Abschlussberichts, (2011).

[51] M. El-Shafie, S. Kambara, Y. Hayakawa, Hydrogen Production Technologies Overview, Journal of Power and Energy Engineering. 07 (2019) 107–154. https://doi.org/10.4236/jpee.2019.71007.

[52] N. Tenhumberg, K. Büker, Ecological and Economic Evaluation of Hydrogen Production by Different Water Electrolysis Technologies, Chem Ing Tech. 92 (2020) 1586–1595. https://doi.org/10.1002/cite.202000090.

[53] T. Smolinka, E.T. Ojong, J. Garche, Hydrogen Production from Renewable Energies-Electrolyzer Technologies, in: Electrochemical Energy Storage for Renewable Sources and Grid Balancing, Elsevier Inc., 2015: pp. 103–128. https://doi.org/10.1016/B978-0-444-62616-5.00008-5.

[54] M. Mehrpooya, F.K. Bahnamiri, S.M.A. Moosavian, Energy analysis and economic evaluation of a new developed integrated process configuration to produce power, hydrogen, and heat, J Clean Prod. 239 (2019) 118042. https://doi.org/10.1016/j.jclepro.2019.118042.

[55] S. Dresp, F. Dionigi, M. Klingenhof, P. Strasser, Direct electrolytic splitting of seawater: Opportunities and challenges, ACS Energy Lett. 4 (2019) 933–942. https://doi.org/10.1021/acsenergylett.9b00220.

[56] F. Giacalone, M. Papapetrou, G. Kosmadakis, A. Tamburini, G. Micale, A. Cipollina, Application of reverse electrodialysis to site-specific types of saline solutions: A techno-economic assessment, Energy. 181 (2019) 532–547. https://doi.org/10.1016/j.energy.2019.05.161.

[57] M. Tedesco, A. Cipollina, A. Tamburini, I.D.L. Bogle, G. Micale, A simulation tool for analysis and design of reverse electrodialysis using concentrated brines, Chemical Engineering Research and Design. 93 (2015) 441–456. https://doi.org/10.1016/j.cherd.2014.05.009.

[58] A. Daniilidis, R. Herber, D.A. Vermaas, Upscale potential and financial feasibility of a reverse electrodialysis power plant, Appl Energy. 119 (2014) 257–265. https://doi.org/10.1016/j.apenergy.2013.12.066.

[59] A. Culcasi, L. Gurreri, A. Cipollina, A. Tamburini, G. Micale, A comprehensive multi-scale model for bipolar membrane electrodialysis (BMED), Chemical Engineering Journal. 437 (2022) 135317. https://doi.org/10.1016/j.cej.2022.135317.

[60] K. Zeng, D. Zhang, Recent progress in alkaline water electrolysis for hydrogen production and applications, Prog Energy Combust Sci. 36 (2010) 307–326. https://doi.org/10.1016/j.pecs.2009.11.002.

[61] P. Millet, Fundamentals of Water Electrolysis, in: Hydrogen Production: By Electrolysis, wiley, 2015: pp. 33–62. https://doi.org/10.1002/9783527676507.ch2.